

Measurements of Heavy Convective Rainfall in the Presence of Hail in Flood-Prone Areas Using an X-Band Polarimetric Radar

SERGEY Y. MATROSOV

Cooperative Institute for Research in Environmental Sciences, University of Colorado, and NOAA/Earth System Research Laboratory, Boulder, Colorado

ROBERT CIFELLI

NOAA/Earth System Research Laboratory, Boulder, Colorado

DAVID GOCHIS

National Center for Atmospheric Research, Boulder, Colorado*

(Manuscript received 14 February 2012, in final form 30 July 2012)

ABSTRACT

The utility of X-band polarimetric radar to provide rainfall estimations with high spatial and temporal resolution in heavy convective precipitation in the presence of hail is explored. A case study involving observations of strong convective cells with a transportable polarimetric X-band radar near Boulder, Colorado, is presented. These cells produced rain–hail mixtures with a significant liquid fraction, causing local flash floods and debris flow in an environmentally sensitive burn area that had been previously affected by wildfire. It is demonstrated that the specific differential phase shift (K_{DP})-based rainfall estimator provided liquid accumulations that were in relatively good agreement with a network of high-density rain gauges and experimental disdrometers. This estimator was also able to capture the significant variability of accumulated rainfall in a relatively small area of interest, and the corresponding results were not significantly affected by hail. Hail presence, however, was a likely reason for significant overestimation of rainfall retrievals for X-band radar approaches that are based on radar-reflectivity Z_e measurements that have been corrected for attenuation in rain. Even greater overestimations were observed with the S-band radar of the weather-service network. In part because of larger range distances, these radar data could not correctly reproduce the spatial variability of rainfall in the burn area.

1. Introduction

The relative compactness and generally low cost of X-band (wavelength $\lambda \approx 3$ cm) scanning polarimetric radars make them a convenient tool for estimating rainfall. (e.g., Matrosov et al. 1999, 2002; Anagnostou et al. 2004). Precipitation estimates from such radars should be particularly valuable in areas where the coverage by conventional precipitation radar or/and gauge networks

[e.g., the Weather Surveillance Radar-1988 Doppler (WSR-88D) network in the United States] is not adequate or lacks the needed spatial and temporal resolution. Since polarimetric approaches allow for correction of partial attenuation of X-band signals in rain, the use of individual radars or small radar networks in this frequency band (Wang and Chandrasekar 2010) is on the rise for different meteorological and hydrological applications in which precipitation information with high spatial and temporal resolution is needed. Such applications include monitoring rainfall in urban areas and in flash-flood-prone regions, especially in complex-terrain regions where ground obstacles severely affect the useful range of data (e.g., Maki et al. 2010; Anagnostou et al. 2010; Matrosov 2010; Schneebeli et al. 2010).

For a number of years, the National Oceanic and Atmospheric Administration's Earth System Research

* The National Center for Atmospheric Research is sponsored by the National Science Foundation.

Corresponding author address: Sergey Matrosov, R/PSD2, 325 Broadway, Boulder, CO 80305.
E-mail: sergey.matrosov@noaa.gov

Laboratory (NOAA ESRL) used its transportable polarimetric hydrometeorological X-band radar (HYDROX), which was upgraded for dual-polarization use in 1997, for studies of wintertime rainfall/snowfall in the American River basin in California's Sierra Nevada. While rainfall in this region is indeed capable of producing local flooding when precipitation events last for many hours, it is predominantly of the stratiform type with pronounced melting layers (e.g., Matrosov et al. 2007) that are readily identifiable using polarimetric technologies. Corresponding mean rain rates for such events rarely exceed $8\text{--}10\text{ mm h}^{-1}$. While some X-band polarimetric radar observations in convective storms have been performed (e.g., Matrosov et al. 2006; Snyder et al. 2010), testing the utility of such radars for providing reliable high-resolution quantitative precipitation estimation (QPE) in heavy rainfall remains an important research topic.

Convective precipitation sometimes contains mixtures of rain and hail. While hail detection is needed for nowcasting severe weather, assessment of rain rates and accumulations in the event of such mixtures is also an important issue because rainfall runoff can cause flash flooding whereas hail is often not an immediate flood hazard since it takes time for hailstones to melt. Power radar measurements (e.g., reflectivity and differential reflectivity) are affected by both raindrops and hailstones, and it is often very difficult (if not impossible) to quantitatively separate signals coming from these hydrometeor types if both are present in the mixture. Although some empirical S-band reflectivity-truncation-threshold levels (e.g., $53\text{--}55\text{ dBZ}$) have been established for use in rainfall retrievals if echo-signal magnitudes exceed these levels, differential-phase-shift radar measurements could be a more robust way to estimate rain rate in the presence of hail (e.g., Aydin et al. 1995). The specific differential phase shift on propagation K_{DP} is primarily influenced by nonspherical raindrops that do not tumble as they fall. On the other hand, this phase shift is not affected very much by hail (e.g., Smyth et al. 1999). Hailstones are usually significantly more spherical than raindrops, and they generally tumble when falling (Balakrishnan and Zrnica 1990).

Aydin et al. (1995) describe a case study of S-band KDP-based rain-rate retrievals in the rain-hail mixture over a single rain gauge. X-band KDP measurements could be more advantageous for such retrievals as differential-phase signals at this frequency band are ~ 3 times as strong as at S band, despite some non-Rayleigh scattering effects (e.g., Matrosov et al. 2006). This article describes an experimental study of high-resolution rainfall QPE measurements using the polarimetric HYDROX radar in convective rainfall containing some hail.

2. Experimental layout

The exploratory tests of the HYDROX radar applicability for QPE in convective rainfall were conducted in July of 2011 near Boulder, Colorado. The meteorological conditions during the midsummer time period in Colorado and other southwestern states are often influenced by the North American monsoon (Adams and Comrie 1997), which can bring significant amounts of moisture to the Colorado Front Range area. The combination of daytime heating and episodically high moisture content values in the atmosphere leads to strong convective activity in the mountain foothills and adjacent plains. This activity frequently results in the afternoon thunderstorms that can be severe and cause local flooding and hail damage.

The HYDROX radar deployment was part of a collaborative effort among the NOAA ESRL, the U.S. Geological Service (USGS), and the National Center for Atmospheric Research (NCAR) to study post-wildland-fire impacts on rainfall runoff production, soil erosion, and debris flow. In September of 2010, a wildfire occurred in the steep terrain of Fourmile Canyon area within the Rocky Mountain foothills region west of Boulder. It was one of the most costly wildfires in Colorado history and destroyed over 160 homes. Much of the vegetation within an area of about 24 km^2 was classified in 2011 by the USGS as either moderately or severely burnt. Following the fire, the Fourmile Canyon region quickly became an area of significant concern to the National Weather Service and local emergency managers because of a perceived increased vulnerability to flash floods and debris flows. Recognizing this potential threat, an ad hoc monitoring and research effort was coordinated among regional radar operators (including the authors), operators of surface meteorological and flood-warning networks, and researchers at the USGS seeking to study hill-slope geomorphological processes.

The NOAA HYDROX radar was deployed at the NOAA Erie-1 site about 20 km northeast of Boulder (Fig. 1). This radar uses the measurement scheme of simultaneous transmission-simultaneous receiving of horizontally and vertically polarized signals and provides measurements of the reflectivity factors on two polarizations (and thus differential reflectivity), the differential phase, and the copolar correlation coefficient. The main characteristics of the radar are given by Matrosov et al. (2005). The perimeter of the Fourmile Canyon burn area and the X-band radar location are also shown in Fig. 1. This figure also shows three representative radar beams in the direction of the burn area. Terrain elevation profiles for these beams are depicted in Fig. 2. In these profiles, the burn area is seen at distances between about 27

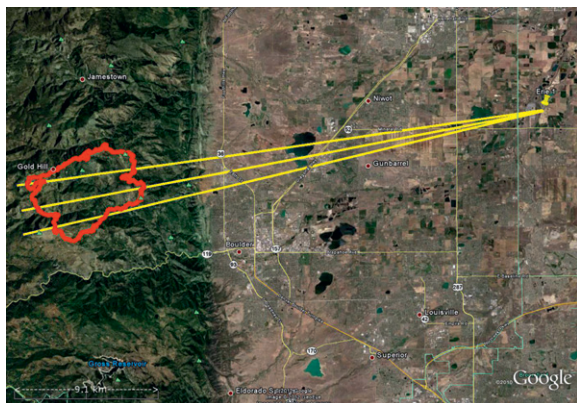


FIG. 1. The study area, with the radar location at Erie-1 and the burn-area perimeter (in red). Radar-beam direction lines for three representative azimuths covering the burn area are shown in yellow. Radar-beam lines are 34.5 km long.

and 34 km from Erie-1. Terrain altitudes inside the burn area varied from about 1.9 to 2.6 km above mean sea level (MSL), while the radar site was located in the plains at an altitude of 1.51 km MSL.

Some ground clutter from the mountainous terrain (Colorado foothills) steeply rising beyond approximately 21 km of range from the radar prevented the use of beam elevation angles of less than $\sim 2.6^{\circ}$ – 3° . Measurements at a 3° radar elevation angle were generally clutter free. With the 3° -elevation pointing geometry, the radar resolution volume is expected to be between approximately 3.0 and 3.55 km MSL (given the beam-width of 0.9°) at a distance of 34.5 km, which corresponds to the left edge of the terrain profiles in Fig. 2. Given this and also judging from the depicted representative terrain profiles, no beam blockage by terrain is expected when radar measurements are taken above the burn area at an elevation angle of 3° [i.e., a 2.55° elevation-angle line of sight corresponding to the lowest beam part would also clear all terrain obstacles in Fig. 2, including Sugarloaf Mountain (2717 m MSL), which is the highest point in the vicinity of the burn area and is located just outside its western boundary].

A special radar scan sequence was devised for this study. This sequence consisted of several sector plan position indicator (PPI) scans in a sector between 150° and 270° and two range–height indicator scans at azimuths pointing toward the middle of the burn area and the nearby Boulder Atmospheric Observatory (BAO) where an impact Joss–Waldvogel disdrometer (JWD; Joss and Waldvogel 1967) was deployed for radar calibration purposes. The whole sequence took 3 min, and it was repeated continuously during radar observation periods. The HYDROX radar beamwidth of 0.9° and the pulse width of $1 \mu\text{s}$ provided a spatial resolution of

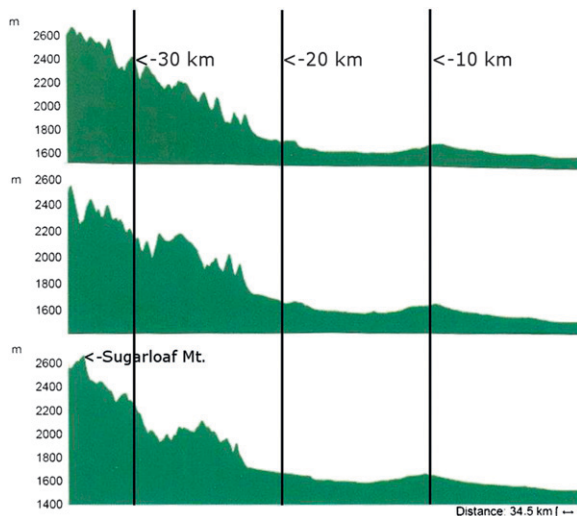


FIG. 2. The terrain elevation profiles along the azimuthal directions shown in yellow in Fig. 1. The panels correspond to the (top) northernmost, (middle) middle, and (bottom) southernmost azimuthal directions in Fig. 1. The right edge of the figure corresponds to the radar location (1510 m MSL).

about 500 m by 150 m (across and along the beam, respectively) in the burn area at mean distance of 32 km from the radar site.

The close-up view of the Fourmile Canyon topographical map is shown in Fig. 3, where the actual burn area is within the red-line perimeter. Locations of different surface measurement sites that were deployed in the study area and its immediate vicinity are also depicted in this figure. The precipitation measuring instrumentation at three NCAR meteorological station sites (site location numbers 2, 3, and 4 in Fig. 3) included optical Particle Size and Velocity (PARSIVEL) optical laser disdrometers, which were originally designed for measuring liquid precipitation but also can identify solid precipitation particles such as hailstones (e.g., Loffler-Mang and Joss 2000), and the Vaisala, Inc., WXT520 weather station sensors (<http://www.vaisala.com/en/products/multiweathersensors/Pages/WXT520.aspx>), which among other meteorological parameters provided acoustic-based measurements of rainfall in terms of total liquid accumulation, rain-rate time series, and event duration. The WXT520 precipitation sensors could be operated in the tipping-bucket-gauge emulation mode. They are also capable of distinguishing hailstones from raindrops on the basis of the acoustic signal of the hydrometeor impact, and they provide evidence of hail presence and its intensity in number of hailstone hits per unit area per hour.

A separate set of rain gauges inside the Fourmile Canyon burn perimeter was installed and maintained by

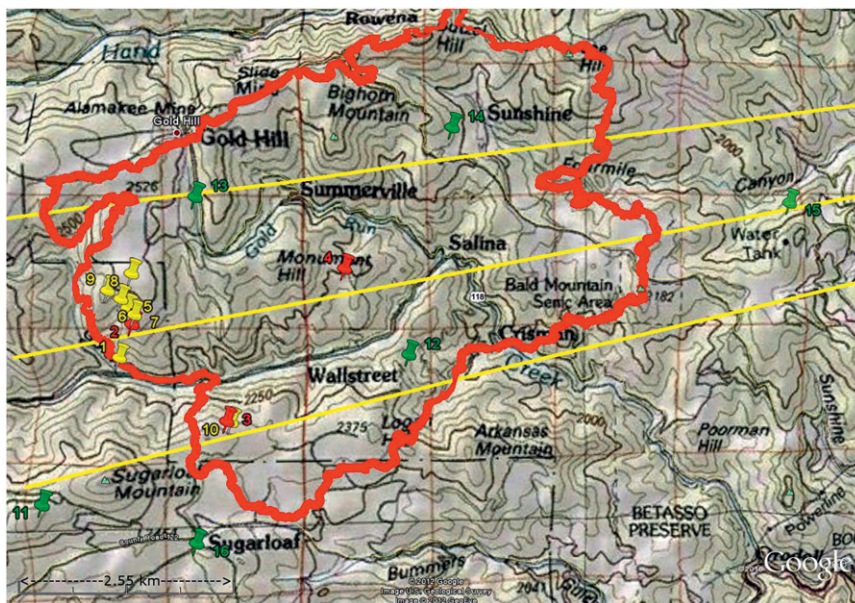


FIG. 3. The close-up view of locations of different surface measurement sites in the Fourmile Canyon burn area and its vicinity. Red indicates NCAR gauge/disdrometer sites, yellow shows USGS gauge sites, and green gives the locations of the ALERT gauge sites. The yellow lines show beam directions from Fig. 1.

the USGS. These gauges were deployed in two areas (sites 1, 5, 6, 7, 8, 9, and 10 in Fig. 3) as part of an intensive study of infiltration and runoff from areas with different burn severity (Moody and Ebel 2012). Additional gauges available for this study were those from the Denver Urban Drainage and Flood Control District [Automated Local Evaluation in Real Time (ALERT)] network (sites 11, 12, 13, 14, 15, and 16 in Fig. 3). These rain gauges are of the standard tipping-bucket type in which the precipitation is observed in a standpipe funnel. Since hailstones (if present) do not melt immediately, it can be expected that these tipping-bucket-type gauges also provide the real-time liquid component of total precipitation.

Some of the ALERT rain gauge sites used in this study were just outside the burn area (i.e., sites 11, 15, and 16) but clearly observed portions of the precipitation event that also generated flooding in the Fourmile Canyon. Although the NCAR, USGS, and ALERT precipitation sensors were different and are used here for QPE comparisons in an ad hoc manner, the combined ground-based network provided a total of 16 surface gauge and gauge-type measurements covering most of the wildfire burn area and allowed estimations of the spatial inhomogeneity of rainfall.

A comparison of Figs. 1 and 3 shows that three radar beams for representative azimuthal angles, which are depicted in Fig. 1, approximately correspond to the directions toward ALERT gauges 13 and 14 (i.e., the northernmost beam in Fig. 1); toward the cluster of

USGS gauges at the western boundary of the burn area, the ALERT gauge 15, and NCAR stations 2 and 4 (i.e., the middle beam in Fig. 1); and toward the ALERT gauges 11 and 12, the USGS gauge 10, and the NCAR station 3 (i.e., the southernmost beam in Fig. 1). Other azimuthal directions covering the burn area (not shown) also suggest that there was no beam blockage by terrain if elevation angles of 3° or above were used for radar measurements.

Radar QPE data over the ground observation sites from 3° elevation-angle measurements used further for comparisons were centered at altitudes from about 2.8 km MSL (for the ALERT gauge 15) to about 3.1 km MSL (for the ALERT gauge 11). Note that the view to ALERT gauge 11 was not blocked by Sugarloaf Mountain even for the 3° beams pointing directly over its summit located at a range of about 34 km from the radar site. The ground QPE measurements at different sites in Fig. 3, correspond to altitudes between about 2.0 and 2.55 km MSL. The vertical difference between radar and ground estimates only slightly exceeds the beam thickness (~ 500 m) at the radar–burn-area slant distances, and no correction of radar data for vertical trends was attempted.

3. Radar observational data and rainfall estimations

The summertime convective monsoon activity in the Colorado Front Range is episodic during July and August.

Observing a “perfect” event is even more difficult if it is sought in a relatively small area such as the instrumented site at the Fourmile Canyon burn. Such an event, however, was observed around midnight on 13/14 July 2011 in universal coordinated time (UTC), which corresponds to 1800 local time, when two intense convective cells moved in close sequence over the burn area from the west-southwest. According to the surface stations, the cells produced heavy rainfall that, during a cumulative period of about 60–70 min, resulted in liquid accumulation varying from around 5 to 35 mm in different parts of the burn area and its immediate vicinity. The presence of hail was also recorded by independent observers and the NCAR disdrometer sensors. Several residents in the vicinity of the Fourmile Canyon area were temporarily evacuated. Local flash floods and debris flows resulted from this precipitation event.

The dense network of surface observations provides a robust validation during this event to evaluate the performance of X-band radar capabilities for QPE with high spatial and temporal resolution in moderate-to-heavy convective rainfall at times coexisting with hail. Of specific interest was assessing whether and how rainfall estimators that are based on differential-phase measurements can provide information on liquid precipitation in rain–hail mixtures and how well the radar estimates can capture the spatial heterogeneity of precipitation observed by the surface gauge network. This is important for many hydrological and societal applications because the rainfall fraction in such rain–hail mixtures is primarily responsible for immediate runoff, flash floods, and debris flows.

a. Rain-rate estimators

Although only two convective cells in close sequence (approximately 45 min between major pulses) impacted the burn area during the event, other cells moved near the radar site during the same event of 13/14 July. One such cell moved over the BAO site located at 6 km from the radar site. This cell did not produce any hail, and the corresponding equivalent reflectivity factors Z_{eh} (hereinafter just reflectivities) did not exceed 50 dBZ. The drop size distributions (DSDs) recorded by the JWD at BAO were used to derive the coefficients in the rain-rate R estimators for X band. It was assumed that the BAO DSDs were also representative for other convective cells observed during the event of 13/14 July.

Figure 4 shows scatterplots among different radar parameters (including K_{DP} , Z_{eh} , specific attenuation on horizontal polarization A_h , and specific differential attenuation A_{DP}) and rain rate calculated by using the observed JWD DSDs. Drop number concentrations n_i for JWD size bins D_{ei} , expressed in the diameters of

equal-volume spheres, were corrected for the undercount of smaller drops because this correction was shown to generally produce DSD-based rainfall accumulations that are in better agreement with rain gauge data (e.g., Matrosov 2010). The following equations, which are the summation versions of integrations over continuous DSD functions (e.g., Bringi and Chandrasekar 2001), were used for calculations:

$$K_{\text{DP}} = (180/\pi)\lambda \sum_i \langle \text{Re}[f_{\text{hh}}(D_{ei}) - f_{\text{vv}}(D_{ei})] \rangle n_i(D_{ei}), \quad (1)$$

$$Z_{\text{eh}} = \lambda^4 \pi^{-5} |(m_w^2 + 2)/(m_w^2 - 1)|^2 \sum_i \langle \sigma_h(D_{ei}) \rangle n_i(D_{ei}), \quad (2)$$

$$A_h = 8.68\lambda \sum_i \langle \text{Im}f_{\text{hh}}(D_{ei}) \rangle n_i(D_{ei}), \quad \text{and} \quad (3)$$

$$A_{\text{DP}} = 8.68\lambda \sum_i \langle \text{Im}[f_{\text{hh}}(D_{ei}) - f_{\text{vv}}(D_{ei})] \rangle n_i(D_{ei}), \quad (4)$$

where f_{hh} and f_{vv} are the elements of the forward-scattering amplitude matrix, σ_h is the backscatter cross section (h and v subscripts refer to horizontal and vertical polarizations, respectively), m_w is the refractive index of water, and the summation is performed over the disdrometer size bins ranging from about 0.035 to 0.55 cm.

It was assumed that drop shapes are satisfactorily described by the oblate spheroid model, and the T-matrix method (Barber and Yeh 1975) was used to compute scattering amplitudes and cross sections. It was also assumed that the radar elevation angle is 3° , the mean drop canting angle in the polarization plane is zero, drop temperature is 10°C , and the canting-angle distribution is Gaussian with an 8° standard deviation (Matrosov 2010). The angular brackets in the equations above represent drop orientation averaging. In the calculations, the drop aspect ratio r –equal-volume diameter D (mm) polynomial approximation ($r = 0.9951 + 0.025 10D - 0.036 44D^2 + 0.005 303D^3 - 0.000 249 2D^4$) suggested by Brandes et al. (2005) was used. Although this approximation was obtained from different earlier experimental data sources, it provides drop aspect ratios that are in relatively good agreement with later more detailed experimental observations of drop shapes obtained from wind-tunnel measurements and from two-dimensional video disdrometer measurements (Thurai et al. 2009).

Besides the power-law relations, Fig. 4 also shows linearized relations between specific differential phase shift on propagation and specific attenuation on

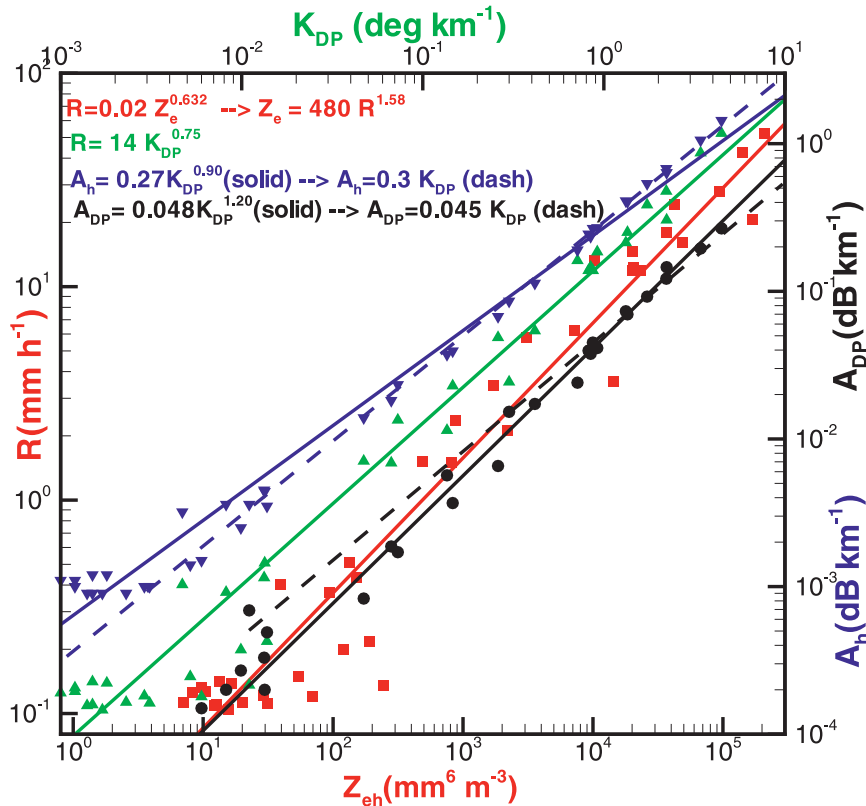


FIG. 4. Color-coded scatterplots and corresponding relations among rain rate and different radar parameters as calculated from DSDs observed during the convective event of 13/14 Jul 2011.

horizontal polarization A_h and specific differential attenuation A_{DP} . The linearized versions of these relations were used to correct HYDROX measurements of reflectivity and differential reflectivity Z_{DR} for rain-attenuation and differential-attenuation effects, correspondingly.

Whereas Z_{eh} - R relations are known for high variations of their coefficients, K_{DP} - R relations usually exhibit more modest variability because K_{DP} and R are proportional to similar moments of the DSD as compared with Z_{eh} and R . The mean X-band K_{DP} - R relation found earlier for Colorado Front Range rains by Matrosov et al. (2006) is R (mm h^{-1}) = $15K_{DP}^{0.76}$ ($^{\circ} \text{km}^{-1}$), which is only slightly different from the best power-law fit $R = 14K_{DP}^{0.75}$ found here for the observational case of 13/14 July 2011.

b. Radar observations

During the routine observations, HYDROX radar power measurements (i.e., Z_{eh} and Z_{DR}) are corrected for attenuation and differential attenuation in rainfall in real time. Figure 5 shows examples of the real-time HYDROX radar sector-scan displays depicting horizontal polarization-corrected reflectivities in the 3°-elevation

PPI scans during observations of the first (0014:30 UTC 14 July 2011) and the second (0051:38 UTC 14 July 2011) convective cells over the Fourmile Canyon burn area. It can be seen that reflectivities at times exceeded 53 dBZ, which is the threshold sometimes used as a hail-presence indicator. Other convective cells with relatively lower reflectivities are seen to the south of the radar site. One of those cells later reached the BAO site, which is also shown in Fig. 5. The JWD data from this rainfall cell were used to derive the relations in Fig. 4.

Figure 6 shows examples of real-time range-height indicator (RHI) measurements through the middle of the burn area (azimuth 259.4°) for the cells mentioned above. The presented RHI scans are close in time to the sector scans shown in Fig. 5. As before, reflectivities corrected for attenuation in rainfall are depicted. It can be seen that echo tops in the middle of the cells reach heights of about 10 km above the ground. The high-reflectivity core regions ($Z_{eh} > 53$ dBZ), which likely included hail, reach heights of several kilometers. The measurements illustrate challenging conditions for QPE when the liquid (i.e., the rainfall) component is of principal interest.

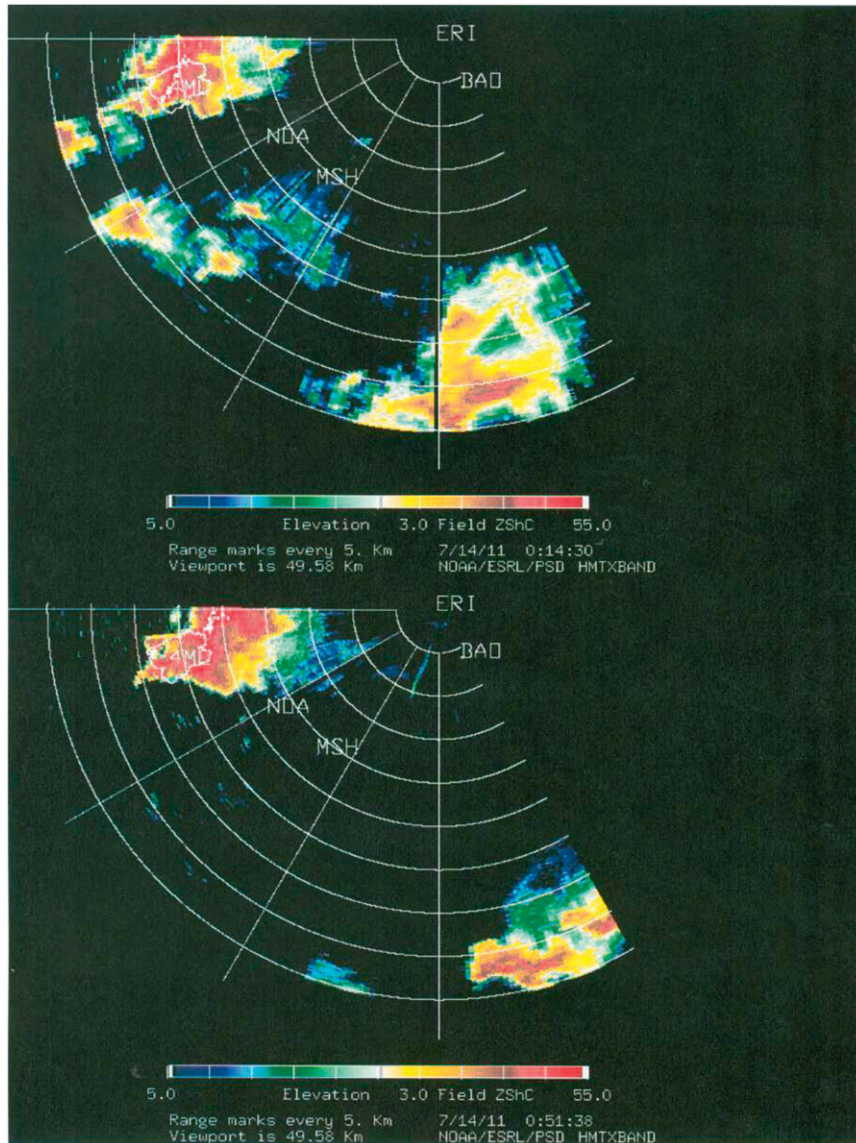


FIG. 5. Examples of real-time HYDROX PPI displays of corrected-for-attenuation Z_{eh} during observations of the (top) first and (bottom) second convective cells over the Fourmile Canyon burn area (the burn-area perimeter is shown in white). Range rings are every 5 km.

4. Radar-based QPE and comparisons with the ground measurements

Rainfall estimates in a rain–hail mixture that are based on power measurements (e.g., Z_{eh} or Z_{DR}) are uncertain and often are significantly biased because hailstone contributions to the total backscatter are often high and difficult (if not impossible in many practical cases) to account for. Attenuation-correction methods for radar power measurements can also provide uncertain results because of reflectivity contributions from hail [for those methods that use attenuated Z_{eh}

measurements, like the “ZPHI” method (e.g., Testud et al. 2000)] and unknown hail attenuations. Wet hail attenuations can also result in underestimation of corrected reflectivities when corrections are obtained by scaling the filtered phase measurements using the linearized relations between attenuation coefficients and specific differential phase shift (as is done in the real-time correction scheme for the HYDROX radar), because these relations are developed for liquid precipitation and assume oblate drop shapes.

As mentioned earlier, rainfall estimates that are based on K_{DP} are expected to perform significantly better

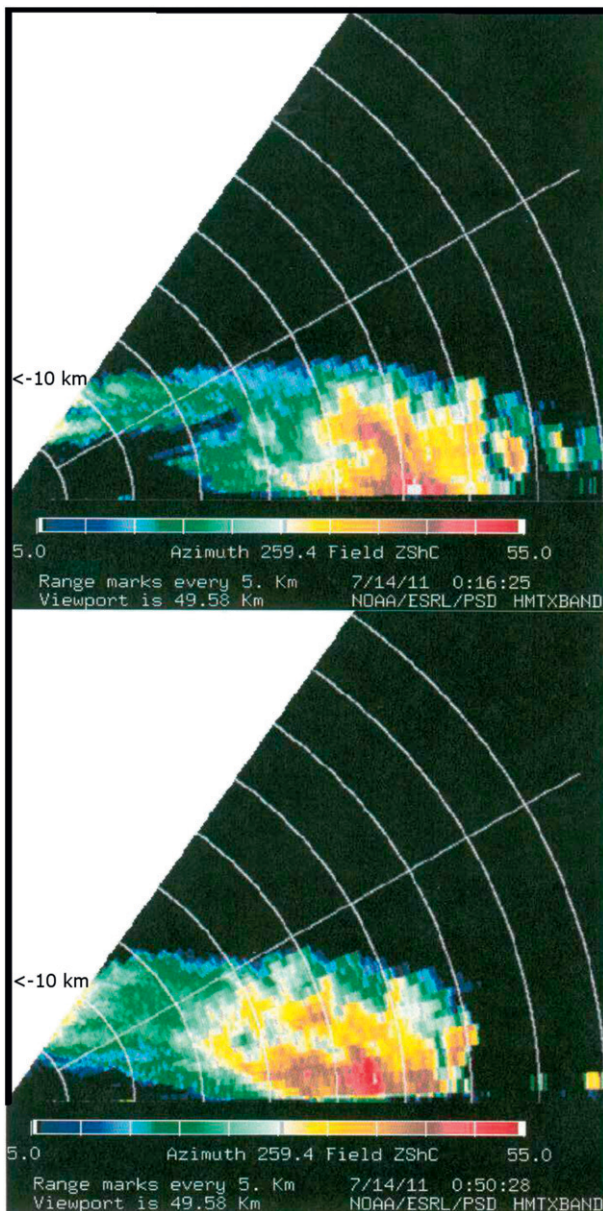


FIG. 6. Examples of real-time HYDROX RHI displays of corrected-for-attenuation Z_{eh} during observations of the (top) first and (bottom) second convective cells over the Fourmile Canyon burn area. Range rings are every 5 km; marks at 10 km above the ground are shown on the vertical axis.

because differential-phase signals are formed mostly by oriented raindrops, and hail contributions to these signals are believed to be small because of more spherical hailstone size and solid particle tumbling during fall (e.g., Balakrishnan and Zrnica 1990; Aydin et al. 1995). Even if large hailstones can be sometimes oblate and aligned, they often make a negligible contribution to specific differential phase shift on propagation, although Z_{DR} can be affected (Smyth et al. 1999). The K_{DP}

estimates obtained as a slope (i.e., the range derivative) of filtered and smoothed differential-phase measurements are also immune to errors in absolute radar calibration and partial signal attenuation (e.g., Zrnica and Ryzhkov 1996). The K_{DP} - R relation discussed in the previous section was used for assessing liquid QPE during the event of 13/14 July 2011.

Figure 7 shows an example of the radar parameters along the beam for an azimuth angle of 259° crossing the middle of the Fourmile Canyon burn area at the time of the scan presented in the upper frame of Fig. 5. For the data in Fig. 7, the convective cell is located between ranges of ~ 25 and 37 km. There is an area of light rain in front (east) of the cell where reflectivities are around 20 dBZ, K_{DP} values are around 0° km^{-1} , and differential-reflectivity values are around 0.2 dB, which is on the order of HYDROX estimated Z_{DR} uncertainties due to measurement noise (Matrosov 2011). Beyond the range of about 25 km, the observed differential phase inside the cell increases very fast. The total increase is about 53° over a 10-km range. Corrected Z_{eh} and Z_{DR} data in Fig. 7 represent values after accounting for attenuation in rain using the filtered phase measurements and the A_h - K_{DP} and A_{DP} - K_{DP} relations shown in Fig. 4.

The observed and filtered differential-phase-shift data are shown in Fig. 7. The observed values Φ_{DP} at a given range gate represent the sum of the phase shift on propagation φ_{DP} accumulated over the whole distance between the radar site and this gate and the backscatter phase shift δ_{hv} at this resolution gate (i.e., $\Phi_{DP} = \varphi_{DP} + \delta_{hv}$). Filtering HYDROX phase data largely removes δ_{hv} contributions from rain and hail and alleviates the influence of the phase measurement noise, so calculations of K_{DP} (as the range derivative of differential-phase data) and attenuation and differential-attenuation corrections are largely based on φ_{DP} estimates. Note that more sophisticated δ_{hv} removal methods, such as those that are based on Z_{DR} - δ_{hv} relations for rain, are not generally applicable to rain-hail mixtures.

The copolar correlation coefficient ρ_{hv} values in the Fig. 7 example are relatively high in the precipitation area, although in the interval between about 31 and 35 km there is a pronounced ρ_{hv} "dip." The power signal-to-noise ratio (SNR) in this interval was about 28, 20, and 13 dB at ranges 31, 33, and 35 km (not shown), so this ρ_{hv} dip is not due to low signal level but rather can be attributed to the influence of tumbling hail (at least between 31 and 33 km where SNR is high) coexisting with rain. This suggestion is also supported by a rapid drop of Z_{DR} between these ranges from values of about 3 dB, which are characteristic of rainfall at these reflectivity levels (i.e., ~ 45 – 50 dBZ), to around 2 dB and lower. The reflectivity decrease beyond the range of

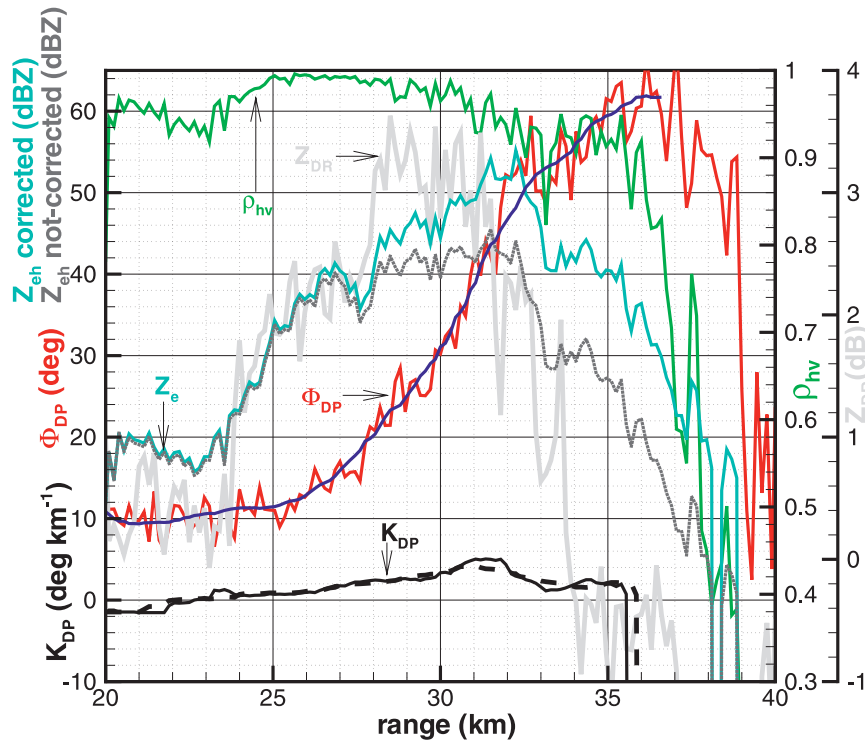


FIG. 7. Observed and filtered differential phase Φ_{DP} (red and blue), copolar correlation coefficient ρ_{nv} (green), observed and corrected-for-attenuation-in-rain reflectivity Z_{eh} (cyan and dark gray), corrected differential reflectivity, Z_{DR} (light gray), and estimates of K_{DP} (solid black for $\Delta x = 3$ km; dashed black for $\Delta x = 4$ km) as a function of range for the radar beam pointed at the azimuth 259° at 0014:09 UTC 14 Jul 2011.

about 32–33 km, which is accompanied by diminishing K_{DP} , might be explained by decreasing the rainfall component in the mixture.

The outer edge of the cell corresponds approximately to 36.5–37 km. The corrected Z_{DR} at this edge is from -0.4 to -0.5 dB rather than the expected 0 dB, which might indicate some “overcorrection.” This overcorrection could be removed if the coefficient in the linearized relation between differential attenuation and differential phase shift on propagation is adjusted from 0.045 km dB^{-1} (see Fig. 4) to about 0.037 km dB^{-1} as some variability in this coefficient due to DSD changes and from event to event is expected. It should be mentioned, however, that correction procedures used here are valid for rain media, and the presence of hail makes them somewhat uncertain. Given this and also because Z_{DR} is not quantitatively used in this rainfall QPE study, no coefficient adjustments were introduced.

Both Φ_{DP} and ρ_{nv} are very noisy outside precipitation regions. The K_{DP} in Fig. 7 is shown for two cases in which two different running-window (filtering) intervals (i.e., $\Delta x = 3$ km and $\Delta x = 4$ km) are used for calculating specific differential phase shift as a range derivative of

filtered and smoothed differential-phase measurements. The longer interval results in smoother K_{DP} values, although the main features are still pronounced at both spatial resolutions.

The HYDROX total rainfall accumulations for the ground validation sites (Fig. 3), as derived for the whole event using the K_{DP} -based estimator, are shown in Fig. 8. The ground-station site numbers are the same in these two figures. The accumulations calculated after the radar rain-rate estimates were linearly interpolated from two consecutive sector scans at the same elevation (i.e., 3°) and selecting the nearest radar resolution gate to each particular validation site. It can be seen that the time intervals of the most rapid rain accumulation generally correspond to about 2345–0015 UTC (i.e., 194.99–195.01 in yearday units) and 0036–0050 UTC (i.e., yearday 195.025–195.035). These are the approximate passing times of the two heavy convective cells.

The K_{DP} -based rain-rate estimator used the relation $R (\text{mm h}^{-1}) = 14K_{DP}^{0.75} (\text{deg km}^{-1})$ when the corrected value of Z_{eh} exceeded a threshold of 31 dBZ. Otherwise, corresponding instantaneous rain rates were calculated using the relation $Z_{eh} (\text{mm}^6 \text{ m}^{-3}) = 480R^{1.58} (\text{mm h}^{-1})$

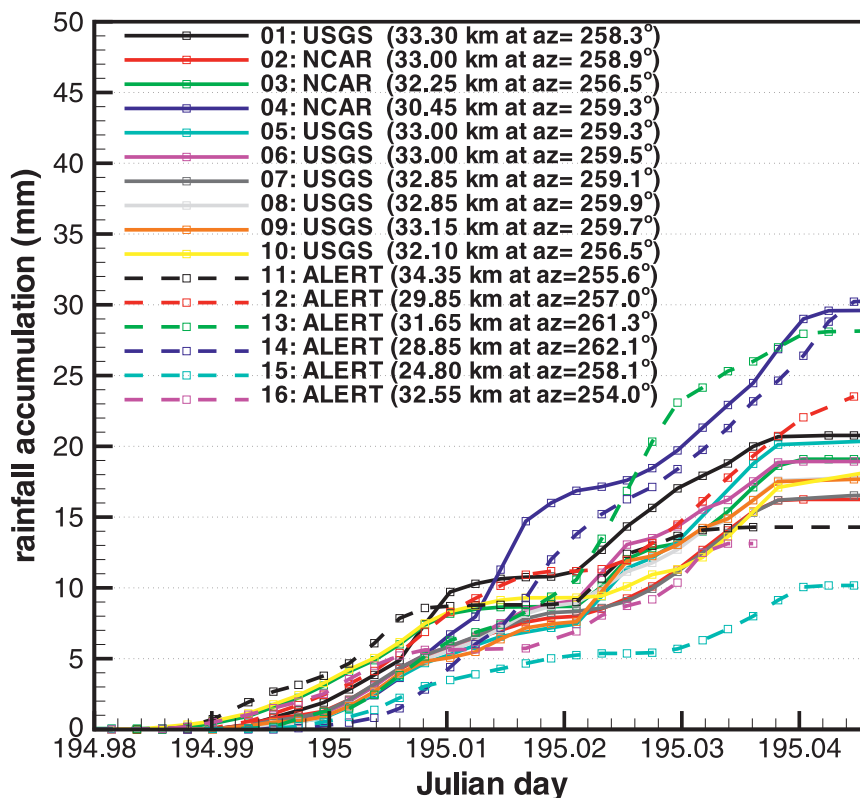


FIG. 8. Rainfall accumulation as a function of time for the event of 13/14 Jul 2011 as retrieved from the K_{DP} -based estimator over the gauges in the Fourmile Canyon burn area.

derived for convective rainfall (see Fig. 4). It can be seen from Fig. 7 that for this example K_{DP} values in precipitation above this threshold are all positive. At lower reflectivities, differential-phase-shift signals become progressively noisier, and K_{DP} -based rain-rate estimates are not very reliable and standard estimators calculating K_{DP} as a slope of differential phase sometimes provide negative values. The threshold 31-dBZ value used in this study is more conservative than has been previously used with HYDROX data (e.g., Matrosov et al. 2006). For the event of 13/14 July in the Fourmile Canyon area, total accumulations overwhelmingly (generally >90%), came from precipitation characterized by Z_{ch} greater than the reflectivity threshold value mentioned above. Thus, the majority of rainfall was estimated using $R(K_{DP})$.

The accumulation estimates, which were based exclusively on corrected reflectivity measurements using the best-fit Z_{ch} - R relation from Fig. 4, provided total rainfall accumulations that exceeded those from the K_{DP} -based estimator by a factor of 1.5–2 depending on the site location. Since the radar reflectivity measurements are expected to be significantly biased by hail, the corresponding accumulations are not shown. For the

same reason the rainfall estimators that use the combination of Z_{ch} and differential reflectivity Z_{DR} were not evaluated.

For comparison purposes, estimates of total rainfall accumulation in the Fourmile Canyon burn area were also performed using available data from the closest WSR-88D located east of Denver at 39.7867°N, 104.5457°W (i.e., about 77 km from the center of the burn area). This radar, which has a four-letter identifier KFTG, was nonpolarimetric at the time of this study, so only reflectivity-based estimates were conducted (corresponding accumulation plots are not shown). Without reflectivity thresholding, the KFTG-based accumulation estimates exceeded the gauge data by a factor of ~3.2 on average, which is, in part, due to the bias by hail. If the standard 53-dBZ threshold is applied to mitigate hail contamination, the bias reduces to a factor of ~2.1, which is also very significant. KFTG radar calibration analyses were beyond the scope of this study.

It can be seen from Fig. 8 that HYDROX estimates of total rainfall accumulation in the burn area and its immediate vicinity varied as a factor of about 3 (from ~10 to 30 mm). While the western part of the area, where the cluster of the USGS gauges was located, received

~16–20 mm during this 70-min-long event, the central and eastern parts (i.e., the radar estimates over sites 4, 12, and 14) received noticeably more rainfall (23–30 mm). Such a heterogeneous spatial distribution in rainfall is important since it results in differing runoff and stream- and debris-flow conditions in different parts of the burn area. Ongoing studies are now seeking to assess the sensitivity of surface runoff to various QPE forcing inputs.

The data shown in Fig. 8 correspond to $\Delta x = 4$ km. Changing the K_{DP} estimation interval to $\Delta x = 3$ km results in only relatively slight change in the total accumulations (typically within a few percentage points), and the corresponding data are not shown. These results indicate that, despite inevitable smoothing of rainfall retrievals when applying differential-phase estimators, they are able to provide information on the spatial inhomogeneity of precipitation even in the relatively compact area of particular interest.

Note also that KFTG estimates could not correctly capture the spatial distribution of rainfall over the burn area, providing, for example, an accumulation variability of less than 20% between the western and central parts of the burn area (the corresponding values were generally between 40 and 52 mm using the 53-dBZ threshold) while the HYDROX and ground based observations indicate the corresponding variability to be approximately a factor of 2. It is believed that the relatively crude KFTG spatial resolution (even in the super-resolution WSR-88D operational mode) in comparison with HYDROX over the burn area contributed to this discrepancy.

A scatterplot of rainfall accumulations from the HYDROX K_{DP} -based estimator and surface-station measurements is shown in Fig. 9. To facilitate comparisons, the ground-site numbers are the same in Figs. 3 and 9. PARSIVEL disdrometer-based estimates are shown for the NCAR station locations. These estimates and the collocated WXT520-based measurements (not shown) were generally within 10%–20%. Both PARSIVEL and WXT520 sensors detected the presence of hail during the event. While the WXT520 data include the number of hailstone hits per unit area, deducing the information on hail rates remains largely uncertain; therefore, no attempt to quantify hail accumulations was made.

Overall, the agreement between radar-derived and surface-station data is very satisfactory. The correlation coefficient between surface-station data and radar estimates above the station sites is about 0.81. The radar estimates varied from 10.1 to 28.3 mm, with a mean value of 19.8 mm. The range of surface-station data was larger (from ~3 to 34 mm), with a mean of 17.3 mm.

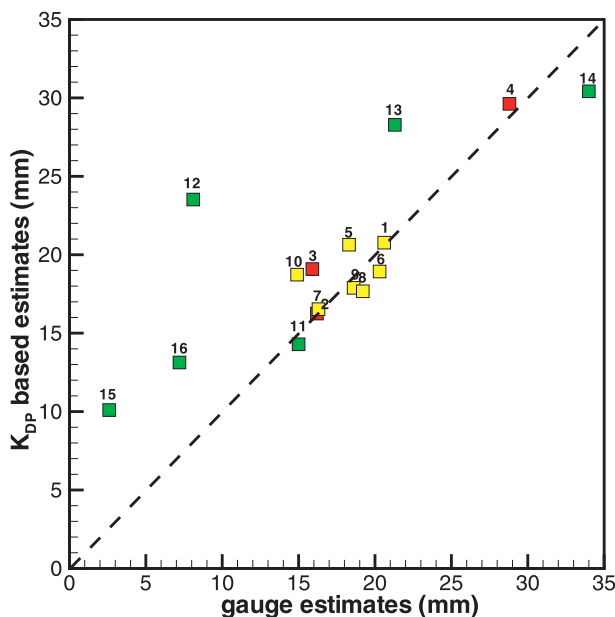


FIG. 9. Comparisons of radar estimates of rainfall accumulation with gauge data for the convective event of 13/14 Jul 2011 in the Fourmile Canyon burn area.

The mean relative bias between these two types of rainfall-accumulation estimates [with the bias being defined as $2(A_r - A_s)/(A_r + A_s)$, where A_r and A_s are accumulations from radar and surface stations, respectively] is about 18%, with radar-derived accumulations being generally higher. Note that tipping-bucket rain gauges tend to underestimate heavy rain rates because of “time to tip” errors when buckets rock frequently back and forth and can underrecord the amount of rainfall (e.g., Allaby 2007). The locations with the largest biases generally correspond to the ALERT gauges while the locations with NCAR disdrometer-based estimates or the USGS tipping-bucket gauge estimates are relatively unbiased. Overall, the agreement is the best in the southwestern part of the area where the cluster of USGS gauges is located. These gauges were calibrated prior to their installation. The information on independent calibration of the ALERT gauges was not available.

Both ground-station and radar data indicate more abundant rainfall in the northern and central parts of the burn area (gauges 4, 13, and 14). While the two convective cells during the event considered here caused significant rainfall in the burn area, the adjacent area to the east of the Fourmile Canyon received significantly less precipitation, as was identified by radar and gauge estimates (e.g., gauge location 15). Rainfall was also minimal in the city of Boulder, which is located about 10 km from the area of interest (see Fig. 1).

5. Discussion and conclusions

The use of polarimetric radars operating at X band for QPE has been steadily increasing during the last 10–12 years. Since radio signals at this frequency band are noticeably attenuated in liquid precipitation, it is expected that the performance of such radars could be more beneficial for light-to-moderate rainfall for which attenuation corrections and deviations from the Rayleigh-scattering regime are relatively small in comparison with heavy-rainfall conditions. The primary objective of this study was to examine the utility of the X-band polarimetric radar measurements for convective-rainfall estimations in an area where liquid precipitation estimations with high spatial and temporal resolution are required.

Of particular interest was assessing the ability of differential phase shift–based measurements to estimate the liquid fraction of precipitation containing a mixture of precipitation types—specifically, rain and hail. The study was performed with the NOAA HYDROX X-band radar observing fast-moving and intense hail-containing convective cells that produced locally heavy rainfall, which, in turn, caused local flash flooding and debris flows in an environmentally sensitive mountainous burn area that was recently affected by severe wildfire. While these cells produced strong radar-signal attenuation, they did not cover the entire observational region. Radar echoes within the radar field of view were not completely extinguished, and a rainfall attenuation-correction procedure could be utilized for radar power measurements.

A rainfall estimator that was based on specific differential phase shift K_{DP} was applied to the HYDROX measurements for calculating liquid precipitation accumulation over 16 surface stations located inside the burn area and its immediate vicinity. Phase-based estimators are immune to the radar absolute calibration, are not significantly affected by partial beam blockage (at least not for severe beam blockages), and are also expected to be relatively immune to the presence of hail in the radar sampling volume (e.g., Zrníc and Ryzhkov 1996). Moreover, the DSD variability affects the K_{DP} – R relations to a lesser extent relative to the Z_e – R relations traditionally used for radar QPE. Although K_{DP} -based rainfall estimates are often noisy (especially at longer radar wavelengths as K_{DP} is proportional to frequency in the Rayleigh-scattering regime) and could be impractical in light rainfall for instantaneous rain-rate retrievals, they are useful for rainfall-accumulation estimates (e.g., Matrosov 2010; Borowska et al. 2011). In heavier rainfall the differential-phase signals are strong and the corresponding K_{DP} values could be reliably derived if the influence of the backscatter phase shift is

removed or largely alleviated. In the presence of hail–rain mixtures, K_{DP} is a convenient tool to infer liquid precipitation fraction. Proper filtering of differential-phase measurements significantly reduces backscatter shift influence induced by larger raindrops and hailstones. Approaches accounting for this phase shift that are based on the use of power radar measurements (e.g., Z_e and/or Z_{DR}) are generally not applicable if hail is present.

For the 70-min-long event of 13/14 July 2011, differential phase–based radar estimates of rainfall indicated that total liquid accumulations over surface validation sites in the burn area and its vicinity varied significantly (generally from 10 to 30 mm). The agreement with surface stations, which measured total liquid accumulation (and detected the presence of hail), was good, with a correlation coefficient of 0.81 and a relative bias of about 18%, which generally is within expected uncertainties of differential phase–based HYDROX estimates (e.g., Matrosov 2010). The gauge errors also can be 10% or even more (e.g., Sieck et al. 2007). The radar estimates were also able to capture the surface-station observed spatial heterogeneity of rainfall accumulation over the burn area, which is important for hydrological applications. Since K_{DP} was conventionally derived as a range derivative of the filtered observed differential phase (and therefore certain smoothing is inevitable), it is encouraging that the radar estimates were able to reveal rainfall heterogeneity in such a relatively small area of the Fourmile Canyon burn area ($\sim 24 \text{ km}^2$).

Unlike for the K_{DP} -based rainfall estimates, the retrievals that are based on reflectivity Z_e measurements, which were not affected by beam blockage over the burn area for the scanning geometry used, revealed a significant overestimation of rainfall accumulation relative to the data from the surface stations deployed in the region of interest. Even with the use of a Z_e – R relation that was specifically derived for similar convective cells and rain-attenuation correction, the corresponding reflectivity-based HYDROX retrievals of rainfall accumulations significantly (by a factor from 1.5 to 2 depending on the surface-station site) overestimated the observed surface-station readings. Such overestimation is explained, in part, by reflectivity contributions from hail, which could not be separated from those by rain in traditional radar measurements. Rainfall accumulations estimated from the closest weather-service radar located at about 77-km range from the burn area (KFTG) revealed even greater biases. KFTG measurements also could not correctly capture the relative differences in accumulation inside the burn area. This fact points to the value of gap-filling radars for rainfall monitoring in relatively small environmentally sensitive areas.

Acknowledgments. The authors acknowledge Kurt Clark for operating and maintaining the HYDROX radar and Carroll Campbell, Jan Gibson, and Tim Coleman for assistance in data processing. The USGS gauge data were provided by John Moody. The ALERT gauge data were provided by the Denver Urban Drainage and Flood Control District. The HYDROX radar operations were supported by the Physical Sciences Division at NOAA ESRL. Support for collection and processing of the NCAR data was provided by Kyoko Ikeda, John Mickey, and Al Jachcik. Support for D. Gochis was provided by the National Science Foundation.

REFERENCES

- Adams, D. K., and A. C. Comrie, 1997: The North American monsoon. *Bull. Amer. Meteor. Soc.*, **78**, 2197–2213.
- Allaby, M., 2007: *Encyclopedia of Weather and Climate*. Facts on File, 832 pp.
- Anagnostou, E. N., M. N. Anagnostou, W. F. Krajewski, A. Kruger, and B. J. Mirovsky, 2004: High-resolution rainfall estimation from X-band polarimetric radar measurements. *J. Hydrometeorol.*, **5**, 110–128.
- Anagnostou, M. N., J. Kalogiros, E. N. Anagnostou, M. Tarolli, A. Papadopoulos, and M. Borga, 2010: Performance evaluation of high-resolution rainfall estimation by X-band dual-polarization radar for flash flood applications in mountainous basins. *J. Hydrol.*, **394**, 4–16.
- Aydin, K., V. N. Bringi, and L. Liu, 1995: Rain rate estimation in the presence of hail using S-band specific differential phase and other radar parameters. *J. Appl. Meteor.*, **34**, 404–410.
- Balakrishnan, N., and D. S. Zrnica, 1990: Estimation of rain and hail rates in mixed-phase precipitation. *J. Atmos. Sci.*, **47**, 565–583.
- Barber, P., and C. Yeh, 1975: Scattering of electromagnetic waves by arbitrarily shaped dielectric bodies. *Appl. Opt.*, **14**, 2864–2872.
- Borowska, L., D. Zrnica, A. Ryzhkov, P. Zhang, and C. Simmer, 2011: Polarimetric estimates of 1-month accumulation of light rain with 3-cm wavelength radar. *J. Hydrometeorol.*, **12**, 1024–1039.
- Brandes, E. A., G. Zhang, and J. Vivekanandan, 2005: Corrigendum. *J. Appl. Meteor.*, **44**, 186.
- Bringi, V. N., and V. Chandrasekar, 2001: *Polarimetric Doppler Weather Radar*. Cambridge University Press, 636 pp.
- Joss, J., and A. Waldvogel, 1967: Ein Spektrograph für Niederschlagsstropfen mit automatischer Auswertung. *Pure Appl. Geophys.*, **68**, 240–246.
- Löffler-Mang, M., and J. Joss, 2000: An optical disdrometer for measuring size and velocity of hydrometeors. *J. Atmos. Oceanic Technol.*, **17**, 130–139.
- Maki, M., and Coauthors, 2010: X-band polarimetric radar network in urban areas. Preprints, *Sixth European Conf. on Radar Meteorology and Hydrology*, Sibiu, Romania, Administratia Nationala de Meteorologie. [Available online at http://www.erad2010.org/pdf/POSTER/Thursday/02_Xband/11_ERAD2010_0354_extended.pdf.]
- Matrosov, S. Y., 2010: Evaluating polarimetric X-band radar rainfall estimators during HMT. *J. Atmos. Oceanic Technol.*, **27**, 122–134.
- , 2011: Polarimetric radar-based estimates of spatial variability in characteristic sizes of raindrops in stratiform rainfall. *J. Appl. Meteor. Climatol.*, **50**, 2514–2525.
- , R. A. Kropfli, R. F. Reinking, and B. E. Martner, 1999: Prospects for measuring rainfall using propagation differential phase in X- and K_a -band radar bands. *J. Appl. Meteor.*, **38**, 766–776.
- , K. A. Clark, B. E. Martner, and A. Tokay, 2002: X-band polarimetric radar measurements of rainfall. *J. Appl. Meteor.*, **41**, 941–952.
- , D. E. Kingsmill, B. E. Martner, and F. M. Ralph, 2005: The utility of X-band polarimetric radar for quantitative estimates of rainfall parameters. *J. Hydrometeorol.*, **6**, 248–262.
- , R. Cifelli, P. C. Kennedy, S. W. Nesbitt, S. A. Rutledge, V. N. Bringi, and B. E. Martner, 2006: A comparative study of rainfall retrievals based on specific differential phase shifts at X- and S-band radar frequencies. *J. Atmos. Oceanic Technol.*, **23**, 952–963.
- , C. A. Clark, and D. A. Kingsmill, 2007: A polarimetric radar approach to identify rain, melting-layer, and snow regions for applying corrections to vertical profiles of reflectivity. *J. Appl. Meteor. Climatol.*, **46**, 154–166.
- Moody, J. A., and B. A. Ebel, 2012: Hyper-dry conditions provide new insights into the cause of extreme floods after wildfire. *Catena*, **93**, 58–63.
- Schneebeil, M., A. Berne, S. Jolivet, X. Muth, J. Jaffrain, N. Daves, and M. Lehning, 2010: Measurements of alpine precipitation with an X-band polarimetric radar and additional sensors. Preprints, *Sixth European Conf. on Radar in Meteorology and Hydrology*, Sibiu, Romania, Administratia Nationala de Meteorologie, P15.14. [Available online at http://www.erad2010.org/pdf/POSTER/Thursday/02_Xband/15_ERAD2010_extended.pdf.]
- Sieck, L. S., S. J. Burges, and M. Steiner, 2007: Challenges in obtaining reliable measurements of point rainfall. *Water Resour. Res.*, **43**, W01420, doi:10.1029/2005WR004519.
- Smyth, T. J., T. M. Blackman, and A. J. Illingworth, 1999: Observations of oblate hail using dual polarization radar and implications for hail-detection schemes. *Quart. J. Roy. Meteor. Soc.*, **125**, 993–1016.
- Snyder, J. C., H. B. Bluestein, G. Zhang, and S. J. Frasier, 2010: Attenuation correction and hydrometeor classification of high resolution, X-band, dual-polarized mobile radar measurements in severe convective storms. *J. Atmos. Oceanic Technol.*, **27**, 1979–2001.
- Testud, J., E. Le Bouar, E. Obligis, and M. Ali-Mehenni, 2000: The rain profiling algorithm applied to polarimetric weather radar. *J. Atmos. Oceanic Technol.*, **17**, 332–356.
- Thurai, M., M. Szakall, V. N. Bringi, K. V. Beard, S. K. Mitra, and S. Borrmann, 2009: Drop shapes and axis ratio distributions: Comparisons between 2D video disdrometer and wind tunnel measurements. *J. Atmos. Oceanic Technol.*, **26**, 1427–1432.
- Wang, Y., and V. Chandrasekar, 2010: Quantitative precipitation estimation in the CASA X-band dual-polarization radar network. *J. Atmos. Oceanic Technol.*, **27**, 1665–1676.
- Zrnica, D. S., and A. Ryzhkov, 1996: Advantages of rain measurements using specific differential phase. *J. Atmos. Oceanic Technol.*, **13**, 454–463.